Coupled identification of the hardening behavior laws and Gurson–Tvergaard–Needleman damage parameters - Validation on tear test of 12NiCr6 CT specimen

Mohamed Hadj Miloud, Ibrahim Zidane, Mohammed Mendas
Laboratoire de Rhéologie et Mécanique LRM, Université Hassiba Benbouali de Chlef, Algeria
m.hadjmiloud@univ-chlef.dz, i.zidane@univ-chlef.dz,m.mendas@univ-chlef.dz

ABSTRACT. This work is devoted to the application of the micromechanical Gurson-Tvergaard-Needleman (GTN) model to study the ductile tearing of 12NiCr6 steel. GTN model is widely used to describe the three stages of ductile tearing: nucleation, growth and the coalescence of micro-voids. A new approach based on the identification of the GTN damage model coupled or not with hardening laws using inverse analysis. After identification, the obtained results show a good agreement between the experimental curve tensile test of an axisymetric notched bar (AN2) and those numerically obtained for GTN model coupled with the hardening laws. In order to validate the identified GTN parameters, a simulation of tear test is conducted on 12 NiCr6 steel CT specimen. The numerical results are compared with experimental results found in the literature and a good agreement is obtained. This identification procedure is more accurate than when the damage parameters are identified independently of the hardening laws.

KEYWORDS. GTN model; Hardening laws; Inverse analysis; FE modeling; VUHARD; ductile fracture.

INTRODUCTION

Many accidental failures of bridges, ships, tanks, pipes, etc., occur that are due to defects generated by: material processing, engineering design process, and the lack of knowledge of some problems as fatigue, corrosion, etc. Scientific researches carried out numerical model/experimental investigations to understand and prevent such accidents. This gave birth of fracture mechanics, which aims to study the propagation of pre-existing cracks within a material. The local approach based on the micromechanical modeling is one of the several methods used in the damage analysis. Numerous models based on a coupling between plasticity and damage has been proposed, notably that of Gurson model [1], which describes the behavior of a porous ductile material. Many variants of this model have been formulated

subsequently [2-4]. The modified Gurson-Tvergaard-Needeleman (GTN) model is widely used in the modeling of ductile fracture. Metallographic studies [5-6] demonstrate that the ductile fracture process of a metal is basically characterized by three mechanisms of void evolution as represented in the Fig. 1.

a) Nucleation of voids due to the debonding of particle–matrix interface, fracture of the particle or micro-cracking of the matrix surrounding the inclusion (Part III);

b) Growth of voids leading to an enlargement of existing cavities (Part IV);

c) Finally, coalescence of micro-cracks initiated from voids leading to the drop of the load-carrying capacity of the material, when the void volume fraction (VVF) reaches to its final value (Part V).

From Fig. 1, we note also that Part I represents the elastic zone and Part II represents the Lüder bands.
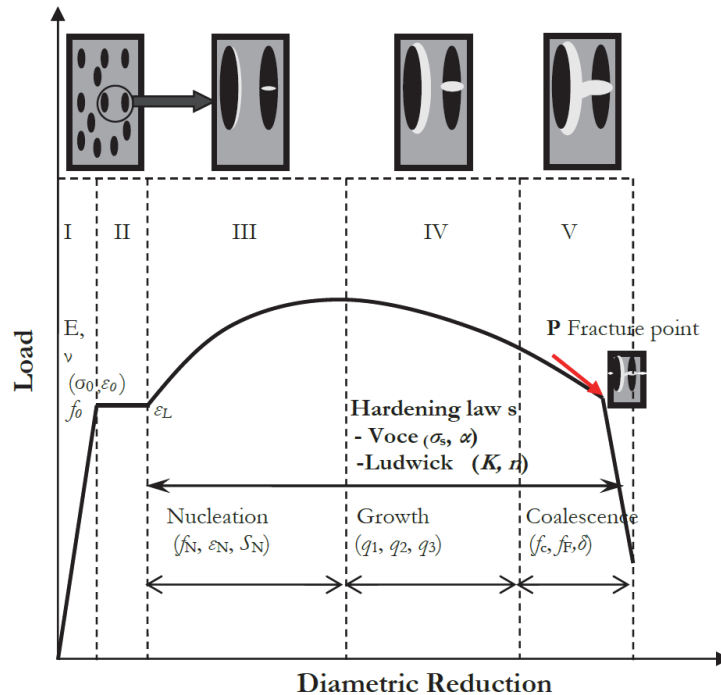

Figure 1: Schematic representation of different stages of ductile fracture.

Gurson [1] developed a constitutive model for porous metal plasticity. This model was derived from an approximated one through an upper bound approach limit-analysis of a hollow sphere made of ideal plastic Mises material. Tvergaard et al. [4] perceived that the Gurson model give adequate results for high triaxiality rates of the stresses but overestimate the fracture strains (ductility) for low triaxialities. Therefore, they introduced the constitutive parameters: q_1, q_2 and q_3 in the Gurson model as:

$$\Phi(\sigma_{eq},\sigma_y,f) = \frac{\sigma_{eq}^2}{\sigma_y^2} + 2\,q_1 f \, cosh\left(\frac{3}{2} q_2 \frac{\sigma_m}{\sigma_y}\right) - \left(1 + q_3 f^2\right) = 0 \tag{1}$$

where: σ_{eq} Von Mises stress, σ_y matrix yield limit, σ_m hydrostatic stress, f the porosity

For the previous yielding criteria and to take into account the fast softening of the material during the coalescence stage (Fig. 1-stage V), Tvergaard and Needleman [2-4] introduced the $f^*(f)$ function. The yield surface of the Gurson-Tvergaard-Needleman (GTN) model is written with the following form:

$$\Phi(\sigma_{eq},\overline{\sigma},f) = \frac{\sigma_{eq}^2}{\overline{\sigma}^2} + 2q_1 f^* \cosh\left(\frac{3}{2} q_2 \frac{\sigma_m}{\overline{\sigma}}\right) - \left(1 + q_1^2 f^{*2}\right) = 0 \tag{2}$$

where: $\overline{\sigma}$ is an equivalent tensile flow stress representing the actual microscopic stress-state in the matrix material, [4].

f^* is the modified porosity follows the law below:

$$f^*(f) = \begin{cases} f & \text{if } f \leq f_C \\ f_C + \delta(f - f_C) & \text{if } f_C < f < f_F \\ f_U^* & \text{if } f \geq f_F \end{cases} \tag{3}$$

with:

$$\delta = \frac{f_U^* - f_C}{f_F - f_C}, \qquad \text{called the coalescence acceleration}$$

f_C is the critical porosity corresponding to the beginning of the coalescence

f_F designate the porosity corresponding to the final fracture of the material.

The ultimo value f_U^* is reached when the macroscopic fracture occurs by loss of the bearing load and is calculated by the following equation $f_U^* = \dfrac{1}{q_1}$ when $q_3 = q_1^2$.

During the plastic flow, the porosity evolution is due to both the voids growth and the voids nucleation:

$$\dot{f} = \dot{f}_{croissance} + \dot{f}_{nucléation} \tag{4}$$

Assuming the matrix incompressibility, the term due to the voids growth is given by the following equation:

$$\dot{f}_{croissance} = (1 - f)\dot{\varepsilon}_{kk}^p \tag{5}$$

$\dot{\varepsilon}_{kk}^p$ is the trace of the macroscopic strain rates tensor. When the nucleation is controlled by the plastic strain, its contribution is as follow:

$$\dot{f}_{nucléation} = A\dot{\overline{\varepsilon}}^p \tag{6}$$

Where $\overline{\varepsilon}^p$ represents the equivalent plastic strain. Chu and Needleman [7] assumed that the priming of the voids follows a normal distribution with a mean strain ε_N and a standard deviation S_N:

$$A = \frac{f_N}{S_N \sqrt{2\pi}} \exp\left[-\frac{1}{2}\left(\frac{\overline{\varepsilon}^p - \varepsilon_N}{S_N}\right)^2\right] \tag{7}$$

The GTN model parameters can be subdivided in three subsets as:
- Constitutive parameters: q_1, q_2 and q_3. Commonly, these parameters are fixed as: q_1=1.5, q_2=1 and q_3= $(q_1)^2$ [2, 8].
- Nucleation parameters: ε_N, S_N and f_N. Generally, the ε_N and S_N values are 0.3 and 0.1 respectively for most materials. Thus, they are considered as constants of the statistical distribution law and not as intrinsic material characteristics. The void volume fraction f_N is the volume fraction of particles available for void nucleation, while the initial void volume fraction f_0 concerns all the inclusions [9, 10].
- The porosities f_0, f_C and f_F are considered as material parameters. The initial VVF parameter f_0 characterizes the initial state of the material. Generally, this parameter is evaluated by microscopic analysis of the undamaged material. For the studied material, the initial void volume fraction f_0 is small (f_0=10^{-5}) [9]. There are several methods to determine the critical void volume fraction f_C. From a physical point of view, there is a threshold of porosity from which the specimen rigidity drops suddenly. But its determination is very difficult. Sun et al. [11-13] have suggested that f_C can be numerically obtained by fitting the numerical curve with the experimental one. The final void volume fraction f_F describes the state of the material at the fracture phase. This parameter is considered as constant and can be determined experimentally [14]. It has been considered as an unimportant parameter, it is interesting to know whether it is a constant Zhang et al. [15]. In this work, the final failure void volume fraction is preset to f_F =0.1.

The critical void volume fraction f_C signifies the onset of coalescence. In most investigations, only the critical void volume fraction f_C is considered as a material parameter. It is obtained by fitting the numerical curves, determined by Finite Element (FE) modeling, with experimental data of notched tensile bar tests [16-21]. A method is proposed for the determination of f_N and f_C, using the experimental fracture strain ε_f [9]. The experimental parameter ε_f is extracted from the load–diametric reduction curve of an axisymmetric notched tensile bar test AN2.

The inverse method is also widely used to identify the GTN-model. In the work of Springmann and Kuna [8, 22], the damage mechanical constitutive laws parameters are identified by locally measured displacement fields and measured force–displacement curves. For the material parameter identification a non-linear optimization algorithm is applied, to render the objective function to a minimum by means of a gradient based method. The force-displacement curves are obtained from tensile tests on notched flat specimens of StE690 steel, which allows the material parameters to be identified [8]. In the work of Jouabi et al. [23], a coupled elastic–plastic/damage is adopted in order to describe tensile behavior with validation on the deep-drawing test of a DP980 Dual Phase steel sheet. The GTN damage model is used. The used hardening laws are those of Swift (non-saturating law), Voce (saturating law) and Hockett-Sherby (saturating law). An identification method for elastic–plastic parameters and GTN damage model parameters has been presented using the software modeFRONTIER [23]. In the literature, there are consistent methods to determine GTN model parameters, but with a pre-defined hardening laws i.e. without identification of hardening laws in the same processes of GTN parameters determination. Recently, many works [24-26] are devoted to identify simultaneously GTN model and hardening laws parameters. Other interesting works of [27 and 28] consist to link the micro-scale to the macro-scale by studying the crack propagation using the GTN model and then determining the R-curves for cracked specimens.

In the first part of this work, we propose a numerical inverse procedure to determine the GTN damage model with and without hardening laws. This procedure is carried out on the software package Abaqus [29]. Within this software, a VUHARD subroutine is implemented to carry out the hardening laws. The experimental data, used in the inverse analysis, are extracted from the load-diametric contraction curve of an axisymmetric notched tensile bar test (AN2) made with 12NiCr6 steel [20]. In the second part, and in order to validate the identified parameters of the GTN model, a numerical simulation of the ductile tear test of a CT25 specimen was performed. The numerical results of the force-displacement curve are compared to those determined experimentally by Wilsius [30].

GTN AND HARDENING PARAMETERS IDENTIFICATION

T he aim of the first step of this work is to identify simultaneously the GTN model and the hardening laws of the 12NiCr6 steel. Hence, a numerical procedure of the inverse analysis, based on the FE method, is used to model the tensile test of an axisymmetric notched bar (Fig. 2). This numerical model is coupled with an optimization tool.
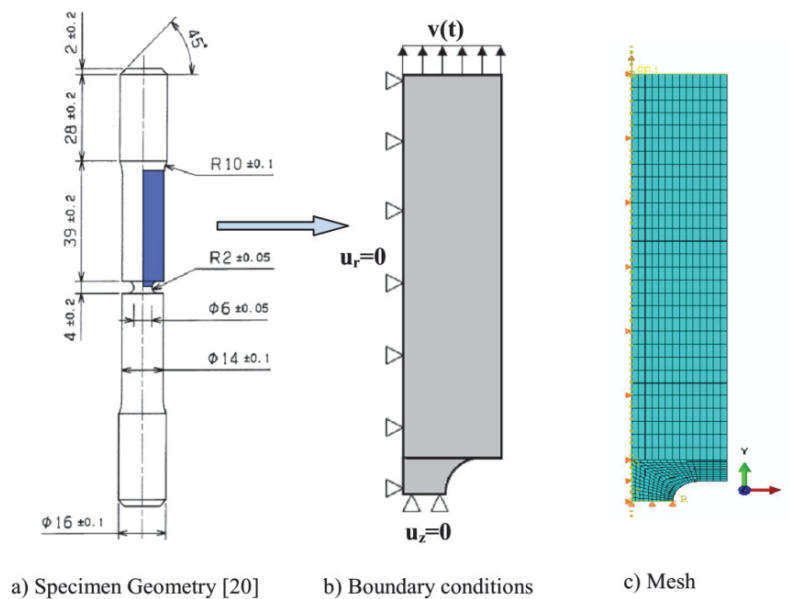

a) Specimen Geometry [20]   b) Boundary conditions   c) Mesh

Figure 2: Specimen geometry and FE model of axisymmetric notched bar with 2 mm radius (AN2).

Tensile tests on notched specimen AN2

The nickel chromium steel used in this investigation is the 12NiCr6 steel. The tensile test was carried out on the notched round tensile bar AN2 [9]. These specimens type have been originally developed for analyzing the hydrostatic stress effect on the failure by ductile tear. The onset necking of those specimens occur at the notch. On this latter a diametric extensometer was set up to measure the diametric reduction. The experimental data obtained from those tests allow to a successful FE identification of damage models [31]. The specimen geometry (Fig. 2-a) and FE model are represented in the Fig. 2-b and c.

FE model of the uniaxial tensile test of AN2.

From the data obtained by [9], the objective is to identify simultaneously the hardening laws and the GTN model of the studied material. The tensile test of AN2 is simulated using the FE software Abaqus/Explicit with taking into account the experimental conditions. In order to compare the numerical results with those experimental obtained in [9], the same specimen dimensions (Fig. 2-a) are considered in the numerical model. Given the symmetry of specimen geometry, only the specimen quarter is modelled in an axis-symmetry case. The quadrilateral elements, type four nodes CAX4R, are used in the meshing. A refined mesh is adapted at the notch zone of the specimen (Fig. 2-c). It should be noted that the element size could be important in FE damage analysis. The number of elements in FE mesh was 660.

A velocity v(t) boundary condition was applied to the top of the FE model (Fig. 2-b). The test was performed in the quasi static case and the same velocity of 0.3mm/min is used in the numerical modelling. The resulting tensile load was determined from nodal forces versus displacement.

The material of the specimen, 12NiCr6, is assumed have an isotropic elasto-plastic behavior. The density of the material is 7.8×10^{-6} Kg /mm^3. The elastic part is described by using Hooke's model with Young's modulus of E=194GPa and a Poisson's ratio of $\nu = 0.3$. For the plastic domain, the von Mises yield criteria is used. It's added to the plastic part of the GTN damage parameters. This model already exists in the software Abaqus/Dynamic Explicit in porous metal plasticity option [29].

In the literature, several formulated laws exist to describe the hardening behaviors from numerous parameters. The adopted laws in this inverse identification procedure are those of Voce and Ludwick. The difference between those laws is that the Voce law is characterized by a saturated yielding stress σ_s for high strains. However, the Ludwick law is characterized by a continuous evolution of the yielding stress. The Lüder bands are taken also into account in the hardening laws following the below equations:

$$\text{Voce Hardening law:} \quad \begin{cases} \text{if} \quad \varepsilon_0 \leq \varepsilon \leq \varepsilon_L & \sigma = \sigma_0 \\ \text{else} \quad \varepsilon > \varepsilon_L & \sigma(\varepsilon) = \sigma_S - \left[(\sigma_S - \sigma_0) \times e^{-(\varepsilon - \varepsilon_L)\alpha} \right] \end{cases} \quad (8)$$

$$\text{Ludwick Hardening law:} \quad \begin{cases} \text{if} \quad \varepsilon_0 \leq \varepsilon \leq \varepsilon_L & \sigma = \sigma_0 \\ \text{else} \quad \varepsilon > \varepsilon_L & \sigma(\varepsilon) = \sigma_0 + \left[K(\varepsilon - \varepsilon_L)^n \right] \end{cases} \quad (9)$$

Where: σ_S saturated yielding stress, σ_0 yielding stress, ε_0 yielding strain, α material dependent adimensioned parameter, K material consistency, n hardening exponent and ε_L strain limit of Lüder bands.

The different behavior laws are implemented through a VUHARD type subroutine in the software Abaqus/dynamic explicit.

Identification strategy

The inverse procedure is used to determine the hardening law and the GTN parameters of studied 12NiCr6 steel, using the numerical model described above. This numerical procedure using the FE model is coupled to an optimization tool in order to minimize the gap between numerical results and experimental data. The optimization tool used « OPTPAR » was developed by Gavrus [32]. The optimal GTN parameters are obtained using the Gauss-Newton iterative algorithm by minimizing the cost function (Q). This tool was widely used in previously research works [32-35] mainly for characterizing the behavior of metallic alloys under static, dynamic, uniaxial and biaxial solicitation. The general scheme of the inverse procedure is shown in the Fig. 3.
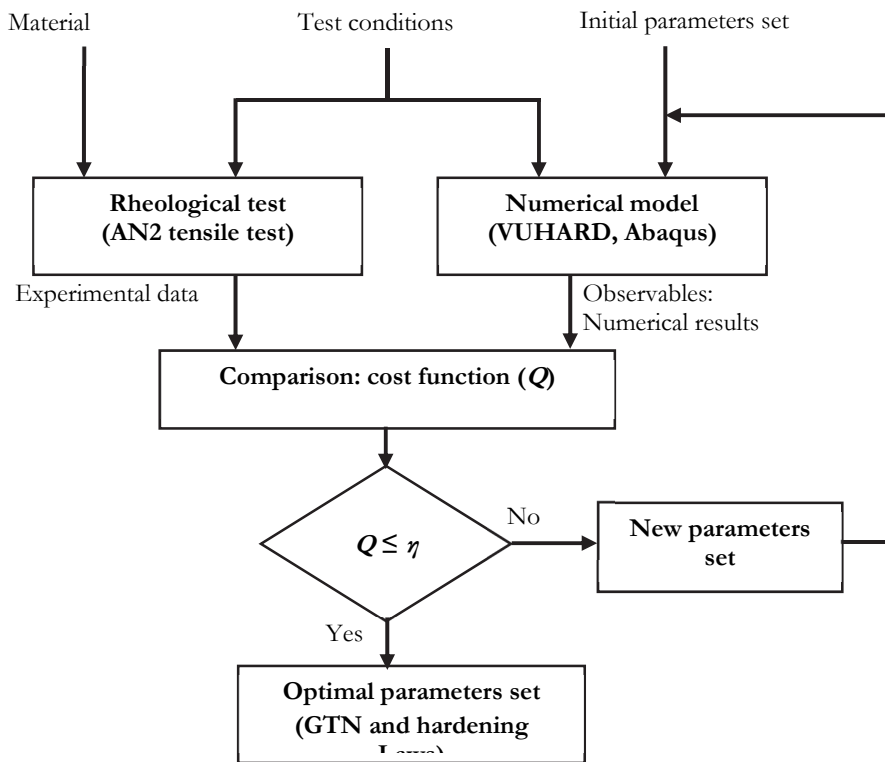
Figure 3: Scheme of identification procedure by inverse analysis.

The cost function to minimize is given by:

$$Q = \frac{\sum_{i=1}^{Np}\left(\overline{F}_{exp}^{i} - \overline{F}_{num}^{i}\right)^{2}}{\sum_{i=1}^{Np}\left(\overline{F}_{exp}^{i}\right)^{2}} \tag{10}$$

with:

$\overline{F}_{exp}$ (or $\overline{F}_{num}$) = { $\overline{F}^{i}$ } with i=1, 2, …

N_p: Total number of experimental measures (or computed),

η: Allowable error.

The numerical/experimental comparison is conducted on the load versus diameter reduction of notched axisymmetric specimen.

Parameters identification procedure

Generally, the determination of GTN model parameters usually consists of a phenomenological procedure which requires a hybrid methodology of comparison between experimental data and numerical results. Hence, the GTN parameters, as it is also indicated in [8, 9, 23 and 31] are obtained by the best fit of the numerical curve with the experimental curve. The nucleation void volume fraction f_N and the critical void volume fraction f_C play a crucial role in the ductile failure process. Thus, the GTN model response is strongly influenced by these two parameters. Then, the identification by inverse analysis will be conducted on the f_N and f_C parameters.

To show the effect of the hardening laws on the GTN parameters identification, in a first step, the GTN model parameters are identified separately of the hardening law $\sigma(\varepsilon)$. The hardening behavior is determined from standard uniaxial tensile test then it is introduced by tabulation in Abaqus (predefined hardening law). Secondly, the two hardening laws are included (Eqs. 8 and 9) in the inverse identification using a VUHARD subroutine coupled with GTN model.

Results and Discussions

Fig. 4 shows the Load-Diametric reduction curve for the notched specimens (AN2) and that obtained from numerical simulation. At the point 'P', there is a sharp change in the slope and drastic fall in load showing the final step of failure process(fracture). The results (Fig. 4 and Tab. 1) present the identification by inverse analysis of the f_N and f_C parameters of GTN model. The plastic behavior part of the material 12NiCr6 is modeled with introducing the experimental hardening curve into the software Abaqus by tabulated form. This hardening curve was obtained from a smooth tensile bar test [30]. The GTN parameters identified do not allow the best description of the fracture point because there is a gap between the experimental and numerical hardening zone of the Load-Diametric Reduction curves. In addition, the fracture point is not clearly observed in the numerical curve.
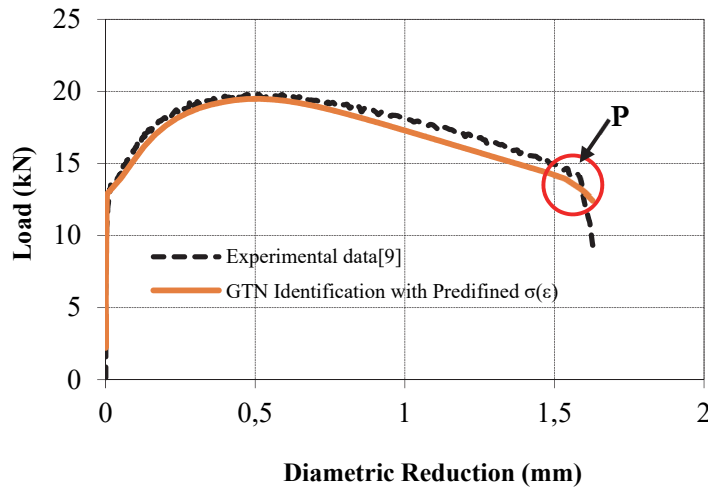

Figure 4: Numerical/experimental comparison of the Load vs. Diametric Reduction curve in the case of GTN model identification with a pre-defined hardening $\sigma(\varepsilon)$.

	Initial parameters	Interval of variation	Identified parameters
Fixed f_F	0.1	0.1	0.1
f_C	0.0100	0.0100 to 0.0800	0.0100
f_N	0.0040	0.0005 to 0.0070	0.0011
Cost function	19.75%	----------------------	5.51%

Table 1: GTN parameters identified with pre-defined $\sigma(\varepsilon)$.

The comparison between identification and experiment of Load/diametric contraction is shown in the Fig. 5 and the Tab. 2. In this identification process, the GTN model is coupled with Voce hardening law. Starting by the hardening parameters, we note that ε_L =0.0214 parameter which characterizes the Lüder bands allows a good representation of the yielding zone. The yielding stress is about σ_0 =339.8 MPa. The plastic parameters of Voce (α =9.380 and σ_S =659MPa) let to a good agreement in hardening zone between experimental and numerical curves. The GTN damage parameters (f_C=0.048 and f_N=0.0065) give the best description of the fracture point 'P' (Fig. 5).

For the following results, the comparison (Fig. 6 and Tab. 3) is done for GTN model coupled with Ludwick hardening law. The strain at the Lüder band limit ε_L =0.026 is close to that identified for Voce law. The yielding stress is about σ_0 =339.8MPa. and it's exactly the same obtained for the Voce law. The plastic parameters of Ludwick (K=428.6MPa and n=0.3) give also a good agreement in hardening zone between numerical and experimental curves. The GTN damage parameters (f_C=0.052 and f_N=0.0088) are also close for the Voce law to describe the fracture point 'P' (Fig. 6).

The results of the used inverse identification are summarized in the Tab. 4. The global comparison between experimental and computed load versus diametric contraction curve is also presented in Fig. 7. We note that the GTN parameters identified (f_C and f_N) with Voce and Ludwick hardening laws are similar to those of the reference [9] and give approximately the same experimental fracture point.
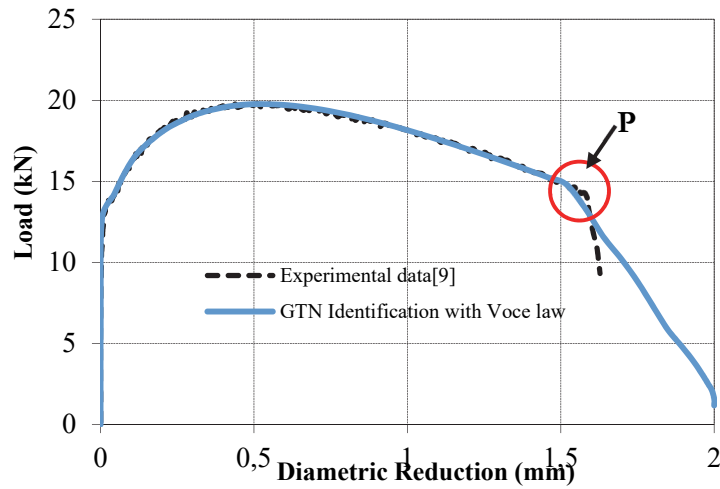
Figure 5: Numerical/experimental comparison of the Load vs. Diametric Reduction curve in the case of the coupled identification of GTN model and Voce hardening law.

	Initial parameters	Interval of variation	Identified parameters
σ_0 (MPa)	420.0	300.0 to 460.0	339.8
α	15.0	5.0 to 70.0	9.38
σ_S (MPa)	800.0	500.0 to 900.0	659
ε_L	0.015	0.01 to 0.05	0.021
Fixed f_F	0.1	0.1	0.1
f_C	0.01	0.005 to 0.08	0.048
f_N	0.004	0.0005 to 0.007	0.0065
Cost function	32.32%	-----------------------	4.01%

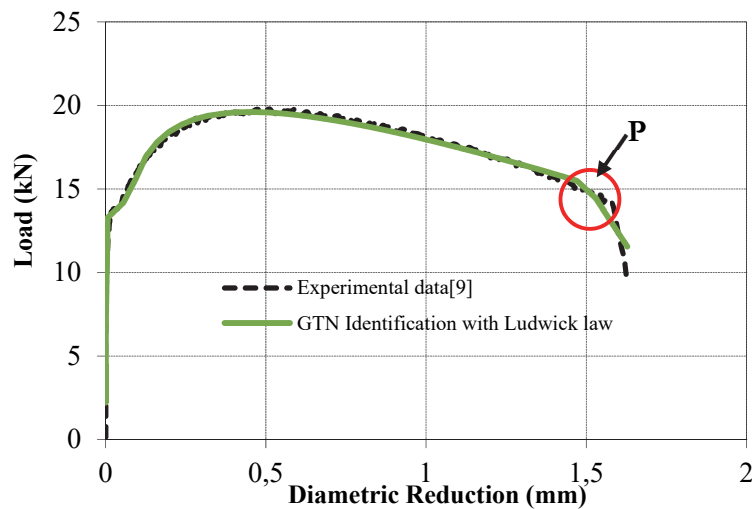Table 2. Identified GTN and Voce parameters.

Figure 6: Numerical/experimental comparison of the Load vs. Diametric Reduction curve in the case of the coupled identification of GTN model and Ludwick hardening law.

	Initial parameters	Interval of variation	Identified parameters
σ_0 (MPa)	420.00	300.0 to 450.0	339.70
K (MPa)	350.00	150.0 to 600.0	428.6
n	0.20	0.150 to 0.50	0.3
ε_L	0.015	0.01 to 0.05	0.026
Fixed f_F	0.1	0.1	0.1
f_C	0.010	0.005 to 0.08	0.052
f_N	0.0040	0.0005 to 0.007	0.0088
Cost function	18%	----------------------	4.13%

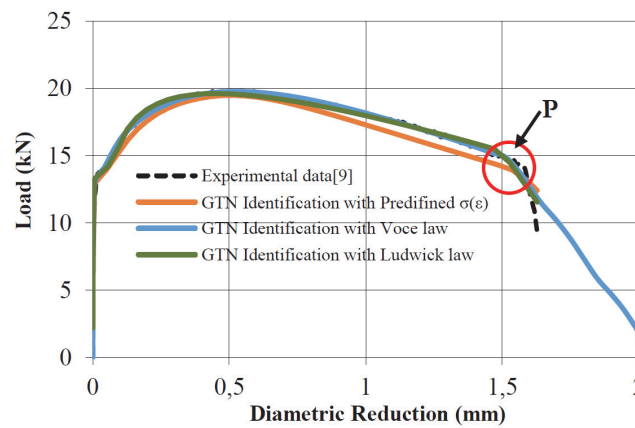Table 3. Identified GTN and Ludwick parameters.

Figure 7: Global comparison between experimental data and numerical results.

	GTN parameters with predefined $\sigma(\varepsilon)$	Voce and GTN parameters	Ludwick and GTN parameters	Ref. [9]
Hardening law	-------	$\sigma_0 =339.8$ MPa	$\sigma_0 =339.7$ MPa	-------
	-------	$\alpha =9.380$	$K = 428.6$ MPa	-------
prameters	-------	$\sigma_S =659$ MPa	$n=0.3$	-------
	-------	$\varepsilon_L =0.0214$	$\varepsilon_L =0.026$	-------
Fixed f_F	0.1	0.1	0.1	0.1
f_C	0.0100	0.048	0.052	0.06
f_N	0.0012	0.0065	0.0088	0.004
Cost function	5.51%	4.01%	4.13%	-------

Table 4. Identified material parameters.

The comparison in the Fig. 7 shows a good agreement between the experimental curve and those obtained for GTN model with Voce and Ludwick hardening laws rather than with predefined hardening σ(ε).

The Fig. 8 presents the evolution of cost function with the iteration number. As it is indicated below, the number of identified parameters, in the case of GTN model identification with tabulated hardening law is lower than the other cases. Therefore, the number of iterations allowing a stagnation of cost function (of 5%) is reached after only two iterations, but low parameters accuracy is observed (Tab. 4). In the two other cases (GTN-Ludwick/Voce) of identification, a high parameters precision is obtained relatively to those found in Ref. [9]. The cost function stagnation is reached after five iterations. We note that, on the one hand, the number of iterations for GTN model identification with predefined σ(ε) is less than with Voce and Ludwick hardening laws, but on the other hand, the obtained parameters are more accurate.
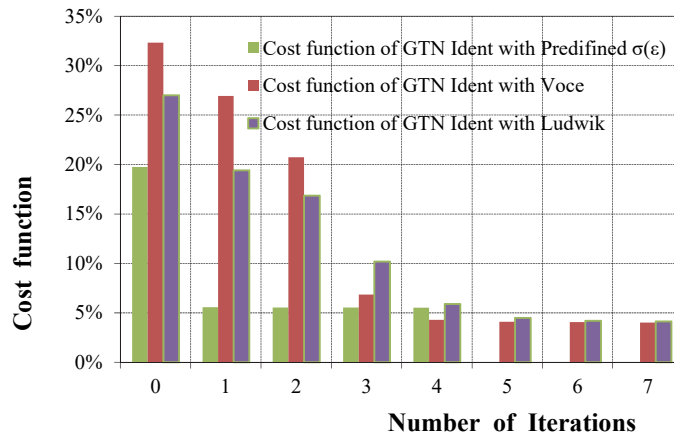
Figure 8: Global comparison between experimental data and numerical results.
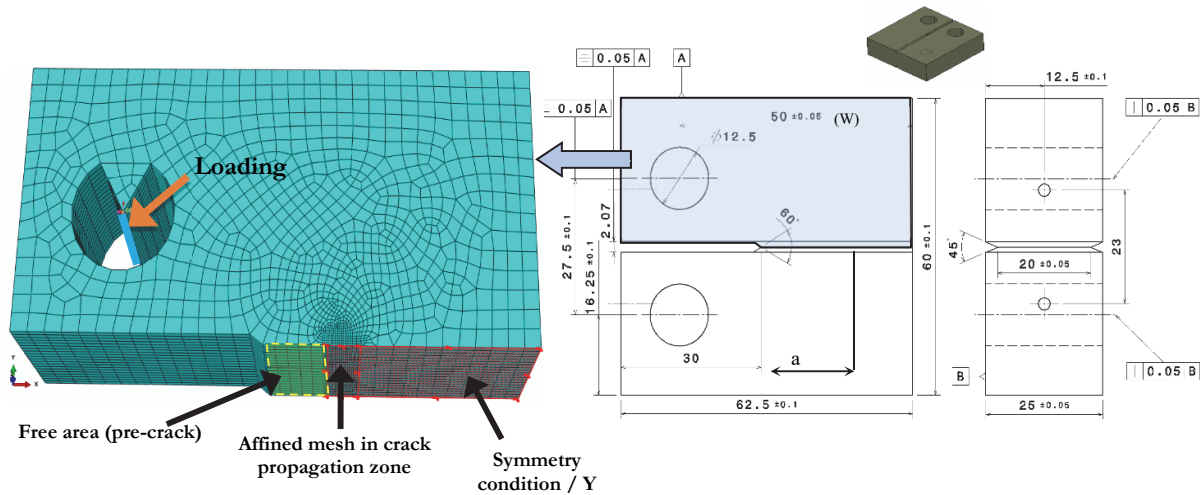

Figure 9: FE model and geometry of the experimental CT25 specimen.

DUCTILE TEAR ON CT SPECIMEN

Experiment

The tear tests were carried out on an Instron-type hydraulic test machine at room temperature on CT specimens pre-cracked (Fig. 9). The test was conducted to reach a ratio $a/W \approx 0.5$, with '*a*' the crack length and '*W*' the specimen width. The CT specimen was pre-cracked by fatigue. After pre-cracking, except one, the specimens were grooved laterally with a depth of 2.5 mm on each side to guide the crack propagation and to have the most rectilinear crack path possible [30]. The tests were carried out under the following experimental conditions:

• Notch opening speed 0.1 mm/min,
• Opening interval of the notch 0.1 mm.

During the test, the loading and the opening of the crack lips were recorded simultaneously. The displacement was measured using a blade extensometer located between the two fixed blades at the front of the specimen [7].

Numerical model

The tear test, described previously, is modeled using the FE software Abaqus/Explicit. In order to compare the numerical results with the experimental data of Ref. [7], the same geometry of the specimen (Fig. 9) is modeled in Cartesian coordinates.

Given the symmetry of the specimen and the use of an isotropic material, only half of the specimen is modeled considering the crack plane as plane of symmetry.

A 3D mesh is adopted and the hexahedral elements, C3D8R type, are used. An affined mesh is adopted in the crack propagation zone of the specimen (Fig. 9). In order to validate the identified GTN model and Voce law by the inverse numerical procedure, the parameters values indicated in Tab. 2 are used in the numerical simulation of the tear test. The loading is applied along a line as shown in the Fig. 9; This represents the pin location where the specimen is loaded. The behavior of this area is considered rigid.

Results and Discussions

Fig. 10 gives the evolution of the applied load as a function of the displacement on the load line for specimens with and without lateral grooves. The obtained results show an experimental dispersion globally caused by the different ratios of pre-crack length a/W according to [30]. The curve corresponding to the test CT1 without lateral notch has a great load than the other specimen. This difference is justified by the difference in thicknesses between the uncut specimen (25 mm) and those with grooves (20 mm). There is an average dispersion of 7 kN between the results of CT tests with grooves. In our opinion, this dispersion is not significant, and it results to the machining effects of the notch. The comparison of the experimental curves with numerical results (Fig. 10: -solid line) shows a good agreement and proves the relevance of the developed numerical model.
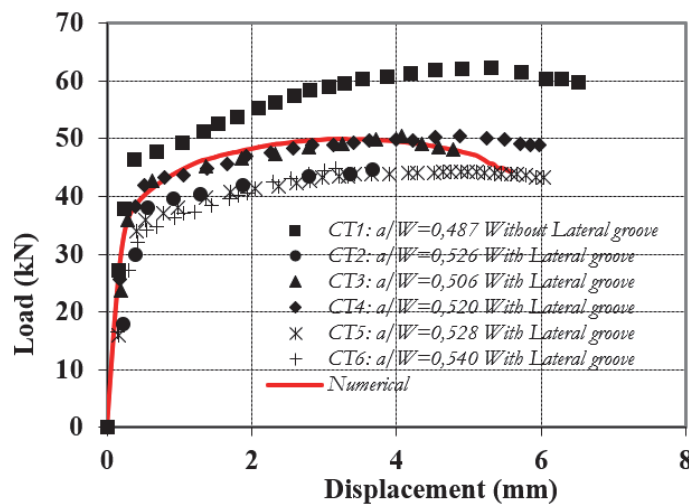

Figure 10: Comparison between Load- displacement curves: experimental [30] and obtained numerical results.

Fig. 11 represents the comparison of the crack propagation observed on the experimental failure facies [30] and that obtained from the numerical results. From this, the crack propagation is materialized by a map of the elements where the final volume fraction is reached f_F =0.1. In our case, when this value f_F equal to 0.1, the element loses completely its rigidity. Both numerical and experimental results are qualitatively comparable and the two fronts show the same aspect of propagation. A well-known crack propagation tunnel phenomenon [30] in the case of plane strains is observed. In fact, when there are no lateral notches, the crack propagation is more developed in the specimen centre rather than at the lateral sides.
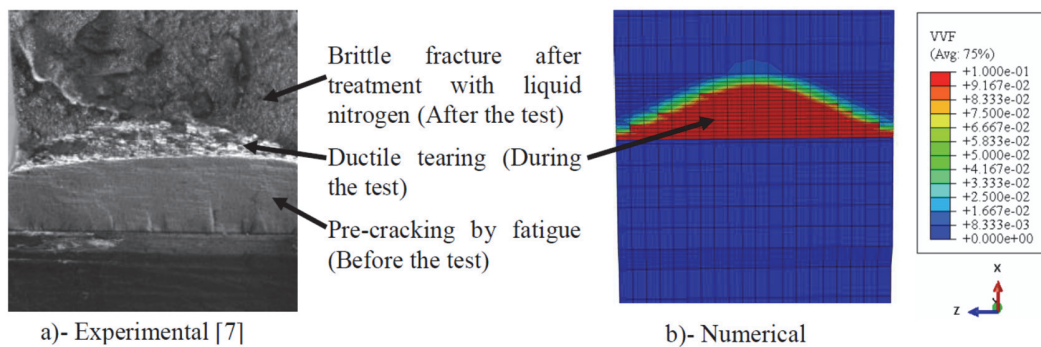

Figure 11: Crack propagation comparison.

CONCLUSION

In this work, an inverse identification procedure is adopted to identify f_N and f_C parameters of GTN damage model coupled with and without hardening laws. The model was built under the software package Abaqus. Despite the high number of parameters, the approach applied made it possible to determine them simultaneously with good accuracy. This is verified comparatively with the experimental results found in the literature.

In the inverse procedure, the experimental results data are extracted from the load-diametric reduction curve of an axisymmetric notched AN2 of 12NiCr6 steel bar tensile test. After identification, we noticed that the identified GTN parameters, f_C and f_N, with Voce or Ludwik hardening law are similar to those of Ref [9] and approximately the same fracture point is obtained. The best fit is obtained with the work hardening law of Voce.

The small difference between numerical results in the case of coupled identification and those obtained experimentally highlights the mutual interaction between the hardening and damage parameters in the mechanical behavior of the materials. Thereafter, the identified GTN parameters are used in the numerical model of tear test on a CT specimen. In order to validate them, the numerical Load-Displacement curve was compared to the experimental results performed by [30]. This comparison shows a good agreement between the experimental and the numerical results. This indicates the relevance of the developed FE model. The crack propagation is materialized numerically by the elements where the final porosity is reached. All of these elements represent the fracture facies profile. In our case, this facies corresponds to that of a CT specimen without grooves. This indicates that it is imperative to take into account the notch in numerical modeling.

REFERENCES

[1] Gurson, A.L. (1977). Continuum theory of ductile rupture by void nucleation and growth: Part I – Yield criteria and flow rules for porous ductile media, J Eng Mater Tech, 99, pp. 2–15. DOI: 10.1115/1.3443401 .

[2] Tvergaard, V. (1981). Influence of voids on shear band instabilities under plane strain conditions, International Journal of Fracture, 17, pp. 389–407. DOI: 10.1007/BF00036191.

[3] Tvergaard, V. (1982). On Localization in Ductile Materials Containing Spherical Voids, International Journal of Fracture, 18, pp. 237–52. DOI: 10.1007/BF00015686.

[4] Tvergaard, V. and Needleman, A. (1984). Analysis of the cup-cone fracture in a round tensile bar, Acta Metallurgica, 32(1), pp. 157–169. DOI: 10.1016/0001-6160(84)90213-X.

[5] Hancock, J.W. and Mackenzie, A.C. (1976). On the mechanisms of ductile failure in high-strength steels subjected to multiaxial stress-states, J Mech Phys Solids, 24(2–3), pp. 147–160. DOI:10.1016/0022-5096(76)90024-7

[6] Thomason, P.F. (1990). Ductile fracture of metals. Oxford: Pergamon Press. https://trove.nla.gov.au/version/20721090

[7] Chu, C. and Needleman, A. (1980). Void nucleation effects in biaxially stretched sheets, Journal of Engineering Materials and Technology,102, pp. 249–56. DOI: 10.1115/1.3224807 .

[8] Springmann, M. and Kuna, M. (2006). Determination of ductile damage parameters by local deformation fields: measurement and simulation, Arch Appl Mech, 75, pp. 775–797. DOI: 10.1007/s00419-006-0033-9

[9] Hadj Miloud, M. Imad, A. Benseddiq, N. Bachir Bouiadjra, B. Bounif, A. and Serier, B. (2013). A numerical analysis of relationship between ductility and nucleation and critical void volume fraction parameters of Gurson– Tvergaard– Needleman model, Proc IMechE Part C: J Mechanical Engineering Science, IMechE, 227(11), pp. 2634–2646. DOI: 10.1177/0954406213476232.

[10] Cox, T. and Low, J.J. (1974). An investigation of the plastic fracture of AISI4340 and 18Nickel-200 grade maraging steels, Metall Trans A, 5, pp. 1457–1470. DOI: 10.1007/BF02646633.

[11] Sun, D.Z., Siegele, D., Voss, B. and Schmitt, W. (1989). Application of local damage models to the numerical analysis of ductile rupture, Fatigue Fract Eng Mater, 12(3), pp. 201–212. DOI: 10.1111/j.1460-2695.1989.tb00527.x.

[12] Sun, D.Z., Siegele, D., Voss, B. and Schmitt, W. (1991). Numerical prediction of ductile fracture resistance behaviour based on micromechanical models, In: JG Blauel and KH Schwalbe(eds) Defect assessment in components – fundamentals and applications (ESIS/EGF9), London: Mechanical Engineering Publications, pp. 447–458.

[13] Sun, D.Z., Kienzler, R,. Voss, B. and Schmitt, W. (1992). Application of micro-mechanical models to the prediction of ductile fracture, fracture mechanics, In: SN Atluri (ed.) 22nd Symposium (II), ASTM STP 1131. Philadelphia, PA: American Society for Testing and Materials, pp. 368–378.

[14] Guillemer-Neel, C., Feaugas, X. and Clavel, M. (2000). Mechanical behavior and damage kinetics in nodular cast iron: Part I. Damage mechanisms, Metall Mater Trans A, 31, pp. 3063–3074. DOI : 10.1007/s11661-000-0085-3.

[15] Zhang, Z.L., Thaulow, C. and Ødegård, J. (2000). A complete Gurson model approach for ductile fracture, Eng Fract Mech, 67, pp. 155–168. DOI: 10.1016/S0013-7944(00)00055-2.

[16] Bernauer, G. and Brocks, W. (1999). Numerical, round robin on micro-mechanical models: conclusions of part A (ductile tearing) and first results of part B (cleavage fracture), In: ESIS TC1 and TC8 meeting, Statoil Research Centre, 26 August.

[17] Oh, C.K. Kim, Y.J. Baek, J.H. Kim, Y.P. and Kim, W. (2007). A phenomenological model of ductile fracture for API X65 steel. Int J Mech Sci, 49, pp. 1399–1412. DOI: 10.1016/j.ijmecsci.2007.03.008.

[18] Pavankumara, T.V. Samala, M.K. et al. (2005). Transferability of fracture parameters from specimens to component level, Int J Press Vessels Pip, 82, pp. 386–399. DOI: 10.1016/j.ijpvp.2004.10.003.

[19] Acharyya, S. and Dhar, S. (2008). A complete GTN model for prediction of ductile failure of pipe, J Mater Sci, 43, pp. 1897–1909. DOI: 10.1007/s10853-007-2369-0 .

[20] Rakin, M., Cvijović, Z., Grabulov, V. and Miloš, K. (2000). Micromechanism of ductile fracture initiation: void nucleation and growth, Facta Univer Ser: Mechanical Engineering; 1(7), pp. 825–833.

[21] Rakin, M., Cvijović, Z., Grabulov, V., Putic, S. and Sedmak, A. (2004). Prediction of ductile fracture initiation using micromechanical analysis, Eng Fract Mech, 71, pp. 813–827. DOI: 10.1016/S0013-7944(03)00013-4.

[22] Springmann, M. and Kuna, M. (2005). Identification of material parameters of the Gurson–Tvergaard–Needleman model by combined experimental and numerical techniques, Computational Materials Science, 33, pp. 501–509. DOI: 10.1016/j.commatsci.2004.09.010.

[23] Djouabi, M. Ati, A. and Manach, P.Y. (2018). Identification strategy influence of elastoplastic behavior law parameters on Gurson–Tvergaard–Needleman damage parameters: Application to DP980 steel, International Journal of Damage Mechanics, 3, 1–28. DOI: 10.1177/1056789518772130.

[24] Zhao, P.J., Chen, Z.H. and Dong, C.F. (2016). Experimental and numerical analysis of micromechanical damage for DP600 steel in fine-blanking process, Journal of Materials Processing Technology, 236, pp. 16–25. DOI: 10.1016/j.jmatprotec.2016.05.002.

[25] Li, H., Yang, H., Lu, R.D. and Fu, M.W. (2016). Coupled modeling of anisotropy variation and damage evolution for high strength steel tubular materials, International Journal of Mechanical Sciences, 105, pp. 41–57. DOI: 10.1016/j.ijmecsci.2015.10.017.

[26] Chen, Y., Zhang, C. and Vare, C. (2017). An extended GTN model for indentation-induced damage, Computational Materials Science, 128, pp. 229–235. DOI: 10.1016/j.commatsci.2016.11.043.

[27] Cricrì, G. (2013). A consistent use of the Gurson-Tvergaard-Needleman damage model for the R-curve calculation, Frattura ed Integrita Strutturale, 24, pp. 161-174. DOI: 10.3221/IGF-ESIS.24.17 .

[28] Sepe, R., Lamanna, G., Caputo, F. (2016). A robust approach for the determination of Gurson model parameters, Frattura ed Integrita Strutturale, 10 (37), pp. 369-381. DOI: 10.3221/IGF-ESIS.37.48.

[29] Abaqus; Version 6.12 (2012). User's manual, Hibbitt, Karlson & Sorensen Inc.

[30] Wilsius, J. (1999). Étude expérimentale et numérique de la déchirure ductile basée sur des approches locales en mécanique de la rupture, PhD Thesis, Université des Sciences et Technologies de Lille, France.

[31] Hadj Miloud, M. (2017). Modélisation de la rupture ductile de l'acier 12NiCr6 par le modèle micromécanique de Gurson, PhD Thesis, UST Oran, Alegria.

[32] Gavrus, A. (1996). Identification automatique des paramètres rhéologiques par analyse inverse, PhD Thesis, Ecole des mines de Paris.

[33] Zidane, I. (2009). Développement d'un banc d'essai de traction biaxiale pour la caractérisation de formabilité et du comportement élastoplastique de tôles métalliques, PhD Thesis, INSA Rennes, France.

[34] Diot, S., Guines, D., Gavrus, A. and Ragneau, E. (2009). Minimization of friction influence on the evaluation of rheological parameters from compression tests – application to a forging steel behavior identification, Journal of Engineering Materials and Technology, 131, pp. 1-10. DOI: 10.1115/1.3026543

[35] Zidane, I., Guines, D., Léotoing, L. and Ragneau, E. (2010). Development of an in-plane biaxial test for forming limit curve (FLC) characterization of metallic sheets, Measurement Science and Technology, 21, 5. DOI: 10.1088/0957-0233/21/5/055701.